Geoscience Frontiers 5 (2014) 877–892

Contents lists available at ScienceDirect

China University of Geosciences (Beijing)

Geoscience Frontiers

journal homepage: www.elsevier.com/locate/gsf

Research paper

Tourmaline from the Archean G.R.Halli gold deposit, Chitradurga greenstone belt, Dharwar craton (India): Implications for the gold metallogeny

Susmita Gupta [a,*], M. Jayananda [b], Fareeduddin [c]

[a] Geological Survey of India (GSI), NER, Guwahati, Assam 781 005, India
[b] Department of Geology, Centre of Advanced Studies, University of Delhi, Delhi 110 007, India
[c] Geochronology and Isotope Geology Division, Central Headquarter, GSI, Kolkata 700 016, India

ARTICLE INFO

Article history:
Received 20 September 2012
Received in revised form
27 November 2013
Accepted 3 December 2013
Available online 10 January 2014

Keywords:
Tourmaline
G.R.Halli
Orogenic gold deposit
Dharwar craton
Archean

ABSTRACT

Tourmaline occurs as a minor but important mineral in the alteration zone of the Archean orogenic gold deposit of Guddadarangavanahalli (G.R.Halli) in the Chitradurga greenstone belt of the western Dharwar craton, southern India. It occurs in the distal alteration halo of the G.R.Halli gold deposit as (a) clusters of very fine grained aggregates which form a minor constituent in the matrix of the altered metabasalt (AMB tourmaline) and (b) in quartz-carbonate veins (vein tourmaline). The vein tourmaline, based upon the association of specific carbonate minerals, is further grouped as (i) albite-tourmaline-ankerite-quartz veins (vein-1 tourmaline) and (ii) albite-tourmaline-calcite-quartz veins (vein-2 tourmaline). Both the AMB tourmaline and the vein tourmalines (vein-1 and vein-2) belong to the alkali group and are classified under schorl-dravite series. Tourmalines occurring in the veins are zoned while the AMB tourmalines are unzoned. Mineral chemistry and discrimination diagrams reveal that cores and rims of the vein tourmalines are distinctly different. Core composition of the vein tourmalines is similar to the composition of the AMB tourmaline. The formation of the AMB tourmaline and cores of the vein tourmalines are proposed to be related to the regional D_1 deformational event associated with the emplacement of the adjoining ca. 2.61 Ga Chitradurga granite whilst rims of the vein tourmalines vis-à-vis gold mineralization is spatially linked to the juvenile magmatic accretion (2.56–2.50 Ga) east of the studied area in the western part of the eastern Dharwar craton.

1. Introduction

Tourmaline is an acentric rhombohedral borosilicate with a general formula expressed as $XY_3Z_6(T_6O_{18})(BO_3)_3V_3W$, where X = Ca, Na, K, vacancy; Y = Li, Mg, Fe^{2+}, Mn^{2+}, Zn, Al, Cr^{3+}, V^{3+}, Fe^{3+}, Ti^{4+}; Z = Mg, Al, Fe^{3+}, Cr^{3+}, V^{3+}; T = Si, Al, B; B = B, vacancy; V = OH, O and W = OH, F, O. The structure of tourmaline is characterized by six-membered tetrahedral rings (T sites) whose apical oxygen atoms point toward the (−) c-pole, producing the acentric nature of the structure. The tourmaline mineral group is chemically one of the most complicated groups of silicate minerals as its composition varies widely because of isomorphic replacement (solid solution).

Boron is an essential constituent of tourmaline. The source of boron can be from fluids or other boron bearing minerals and must be concentrated by geochemical processes in order to form tourmaline, as it is a trace constituent in the upper crust, lower crust and mantle. Formation of tourmaline is strongly influenced by boron content within the protolith and fluids interacting with crustal rocks during metamorphism (Henry and Dutrow, 1996). Tourmaline not only acts as a recorder of boron influx in the rock systems but also records large numbers of inter and intra-site substitution under pressure and temperature conditions ranging from diagenesis to granulite facies and crustal anatexis (Henry and

* Corresponding author. Tel.: +91 9508788394.
E-mail address: susmita_710@yahoo.com (S. Gupta).

Peer-review under responsibility of China University of Geosciences (Beijing)

Production and hosting by Elsevier

1674-9871/$ – see front matter © 2014, China University of Geosciences (Beijing) and Peking University. Production and hosting by Elsevier B.V. All rights reserved.
http://dx.doi.org/10.1016/j.gsf.2013.12.004

Dutrow, 1996). Therefore tourmaline is an unique mineral to document the mineral recrystallization events and fluid flow almost across the entire spectrum of metamorphism. Besides it is a typical accessory mineral in magmatic and sedimentary rocks. For many years, efforts are being made to utilize the tourmaline chemistry for exploration guide as a metallogenic indicator. Tourmaline are reported throughout the world as an important gangue mineral in metallic and non-metallic ore deposits where it occurs either as trace or minor mineral in the host litho-units or as major constituents (>15%) in concordant and discordant layers referred as tourmalinites. The presence of tourmaline is reported worldwide from various gold deposits and it forms an important mineral in many of the Archean orogenic and Proterozoic gold deposits. It also occurs as an accessory gangue mineral in several types of strata-bound gold deposits. Economically, the Au-tourmaline veins are the most valuable, as they form some of the largest and richest gold deposits of the world (Slack, 1996). Tourmaline bearing Au-quartz veins commonly occur within greenschist or amphibolite grade metavolcanic and metasedimentary rocks (and some metaplutonic rocks), especially in the Archean greenstone belts (Roberts, 1987; Hodgson, 1993; Hutchinson, 1993; Ram Mohan et al., 2008).

Tourmaline is spatially associated with greenstone volcanic as well as gold and other ore deposits of India across the geological period. Recently geochemistry of tourmaline is being utilized as a metallogenic indicator (Fareeduddin et al., 2010). Krienitz et al. (2008) reported the presence of tourmaline as minor but widespread constituent in the inner and distal hydrothermal alteration zones of Hira Buddini gold deposit in the Archean Hutti-Maski greenstone belt of the eastern Dharwar craton (EDC). Occurrence of tourmaline is also noted in Kolar gold deposit, Dharwar craton (Siva Siddaiah and Rajamani, 1989). Honnamaradi gold mineralization (nearly 22 km north of present study area) in the Chitradurga greenstone belt (CGB) is marked by intense development of tourmaline (Mohakul and Babu, 2001). Tourmaline occurs as a minor but important mineral in the alteration zone of Archean orogenic Guddadarangavanahalli (G.R.Halli) gold deposit in the CGB of the western Dharwar craton (WDC). No attempt has been made so far to characterize tourmaline for detailed petrography and chemical composition. This paper documents mineralogy and chemical composition of tourmaline and the new dataset is used to discuss the origin of tourmaline and its genetic link with gold mineralization.

2. Geological background

2.1. Regional geology

The Dharwar craton corresponds to a large tilted section of the Archean continental crust that exposes >3.0 Ga old tonalitic-trondhjemitic-granodioritic (TTG) gneisses (commonly known as Peninsular Gneissic Complex or PGC), two generations of greenstone sequences, potassic to calc-alkaline granitoids with synplutonic mafic dykes and mafic dyke swarms (Bhaskar Rao et al., 1992; Chadwick et al., 2000; Jayananda et al., 2000, 2006, 2008, 2013). The craton is divided into two sub-blocks i.e. the western Dharwar and the eastern Dharwar based upon the differences in the nature and abundance of the greenstones and in the degree of regional metamorphism (Swami Nath et al., 1976; Rollinson et al., 1981), plutonism and geochronological studies (Jayananda et al., 2006). The western block is dominated by old TTG (>3.0 Ga) with abundant greenstone sequences and discrete 2.62 Ga potassic plutons whilst eastern block contains younger gneisses with large remnants of old TTG (>3.0 Ga) with thin elongated volcanic dominated greenstone sequences and most voluminous 2.56–2.52 Ga granitoids/diatexites (Jayananda et al., 2013 and references therein). Recently a threefold subdivision is proposed for the Dharwar craton based upon U-Pb zircon ages and Nd isotope data i.e., the WDC with dominant old crust (3.4–3.2 Ga), the central Dharwar craton (CDC) with mixed old and younger crust (3.4–3.2 Ga and 2.56–2.52 Ga) and the EDC with mainly younger (2.7–2.52 Ga) crust (Dey, 2013; Peucat et al., 2013). In this paper we follow the two fold classification of the Dharwar craton.

The boundary between two cratonic blocks is marked by a 400 km long NW–SE trending mylonitic shear zone located on the eastern margin of the CGB (Swami Nath and Ramakrishnan, 1981; Drury et al., 1983; Chadwick et al., 1997) known as the Chitradurga eastern boundary shear zone (CBSZ). The intrusive granite plutons on both side of the CBSZ are entirely different with respect to their pristine and tectonothermal signature (Jayananda et al., 2006; Chardon et al., 2011). The WDC granitoids are emplaced around 2.62 Ga and synkinematic with respect to development of dome-basin patterns associated with D_1 deformation whereas the 2.56–2.52 Ga granitoid plutons in the EDC are emplaced during development of regional strike-slip shearing (Jayananda et al., 2006; Chardon et al., 2011). Late Archean tectono-plutonism between 2.56 and 2.50 Ga accompanied regional HT-LP metamorphism and ended with the formation of massive charnockites from gneisses and migmatites in the deepest exposed crust. The low temperature WDC with dominant development of Mesoarchean to Neoarchean granite greenstone terrains has presumably developed as a fore land over which high temperature EDC with profuse end Archean granitoids and linear greenstone belts are thrusted and amalgamated during the Dharwar orogeny (Chadwick et al., 2000).

2.2. Geology of the Chitradurga greenstone belt (CGB)

The N–S to NNW–SSE trending CGB (Sheshadri et al., 1981) extending for about 460 km long and 2–40 km wide (Fig. 1) is one of the most prominent Achaean tectonic features of the Indian Precambrian terrain. It comprises about 2–10 km thick sequence of metasediments and metavolcanics belonging to the Dharwar Supergroup. The Dharwar Supergroup is grouped into two subgroups viz. older Bababudan Group and younger Chitradurga Group (Swami Nath et al., 1976). The generalized litho-stratigraphic sequence of the eastern part of the WDC is presented in Table 1. The CGB shows a progressive increase in metamorphic P-T conditions from greenschist facies in the north to amphibolites facies in the south (Raase et al., 1986) which coincide with late D_1 and early D_2 events (Mukhopadhyay, 1986). The regional structure of the CGB has been described as second generation central anticline flanked by first generation synclines on either side (Mukhopadhyay et al., 1981; Mukhopadhyay and Ghosh, 1983; Mukhopadhyay and Baral, 1985). These structures are refolded along E–W trending warps formed during D_3 deformation (Mukhopadhyay and Baral, 1985). The D_2 deformation is related with the development of N–S sinistral shear zones within and at the margins of the schist belts (Chadwick et al., 2000) and these shear zones are known for hosting big and small gold deposits in the Dharwar craton. Twenty six gold incidences in different host rocks of the CGB are reported along the eastern extremity of the CGB and in proximity to the CBSZ (Radhakrishna and Curtis, 1999). Three most important gold deposits occurring along the close proximity of the CBSZ are Ajjanahalli, G.R.Halli and Gadag. The CGB, also known for its copper and iron mineralization, is interpreted to have formed as a result of collision tectonics and closure of a basin between two juvenile continental crust blocks (Naqvi, 1985).

2.3. Geology of the G.R.Halli gold deposit

The G.R.Halli (latitude 14°17′00″ N, longitude 76°24′00″ E) gold deposit is located at about 6.5 km north of the Chitradurga town in

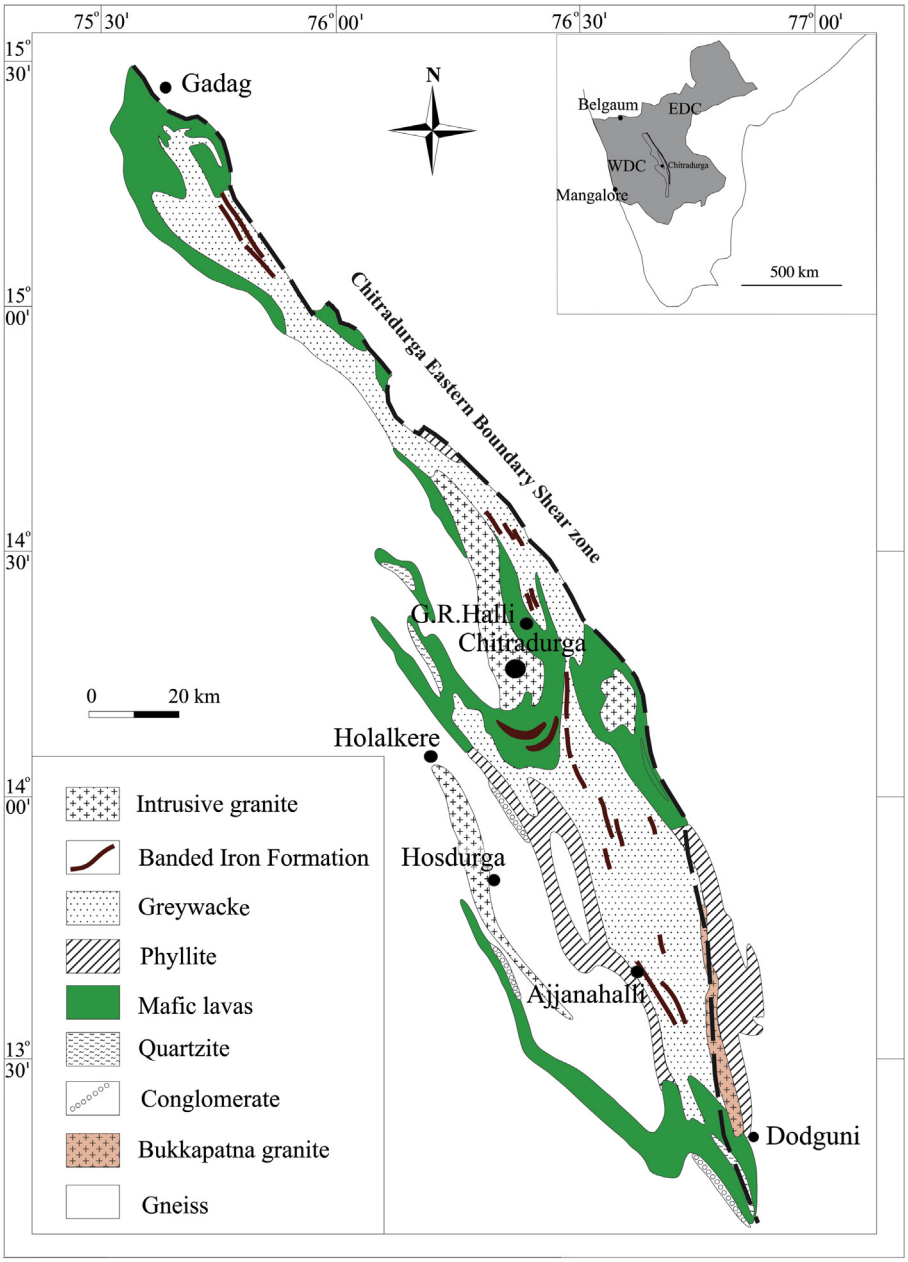

Figure 1. Geological map of the CGB (modified after Jayananda et al., 2011a, b; Radhakrishna and Vaidhyanadhan, 2011) showing the CBSZ and locations of Ajjanahalli, G.R.Halli and Gadag gold deposits. The inset map shows the location of the CGB in Dharwar craton (grey shaded area).

the eastern arm of the Chitradurga anticline (Fig. 2). The surrounding area of G.R.Halli comprises rocks of the Ingaldhal Formation of the Chitradurga Group (2.9–2.55 Ga). To the east G.R.Halli conglomerate separates the rocks of the Hiriyur Formation, to the farther east the basement TTG is exposed. The Chitradurga Granites border the area in the west. Presence of high strain zone or shear zone is documented within the central part of the CGB and very close to the G.R.Halli gold deposit roughly along the contact of metabasalt and metasedimentary units and subparallel to the CBSZ. This is referred as shear corridor (Khan, 2001), Chitradurga Central Shear Zone or CCSZ (Mohakul and Babu, 2001) and Medikeripura high-strain zone or MHZ (Chadwick et al., 2007; Fig. 2). Greyish-green, massive to schistose metabasalt intercalated with greywacke and meta-argillite/phyllite constitute the major litho-units in the studied area. These are intruded by metabasic dyke and sills, quartz-carbonate veins, quartz veins etc. The unaltered/less altered massive metabasalt exposed towards the west of the G.R.Halli village is considered as the base unit to demarcate the wall rock alteration zone. Field and petrographic description of the major litho-units of the area is summarized below.

2.3.1. *Metabasalt (unaltered/less altered)*

The rock is dark greyish, fine grained, massive and consisting of plagioclase laths and altered pyroxene with minor chlorite, ankerite and quartz. Fine laths of plagioclase form triangular spaces, occupied by augite and define intergranular texture. Ankerite grains occur as dissemination. Secondary quartz grains occur as anhedral aggregates. It is associated with minor ankerite and chlorite, possibly representing vesicular filling. Very fine dissemination of pyrite, pyrrhotite and chalcopyrite are ubiquitous.

Table 1
Generalized litho-stratigraphic sequence of the eastern part of the WDC.

	Group	Formation	Lithology
			<2.5 Ga Mafic dykes
			~2.5–2.6 Ga younger granite
Dharwar Supergroup	Chitradurga Group (2.7–2.6 Ga)	Hiriyur Formation	Greywacke-argillite suite with the basic intermediate volcanic, banded ferruginous and polymictic conglomerate (G. R. Halli, K. M. Kere etc.)
			~~
			Disconformity~~~~~~~~~~~~~~~~~~
		Ingaldhal Formation	Basic, intermediate, acid lava and pyroclastics with interbeds of banded pyritiferrous chert and argillite.
		Vanivilas Formation	Chloritic phyllite, banded ferruginous chert, manganiferous chert, phyllite, limestone, dolomite, chlorite-biotite ± garnet phyllite, quartzite, quartz schist, polymictic (Talya) conglomerate.
			~~
			Unconformity~~~~~~~~~~~~~~~~~~
	Bababudan Group (2.9–2.7 Ga)	Mulaingiri Formation	BIF and carbonaceous phyllites, basalts with minor ultramafics
		Santaveri Formation	Acid volcanic, basic to intermediate volcanic, quartzites
		Allampur Formation	Metapyroxenite and metagabbro, quartzite
		Kalasapura Formation	Basic volcanic with associated sediments, quartz-muscovite schist, quartzite, Nerlakatte conglomerate
~~Unconformity~~~~~~~~~~~~			
Younger PGC (3.4–2.9 Ga)			TTG remnants, migmatites and granodiorite gneisses, juvenile granite
Sargur complex (>3.3 Ga)			Komatiite, tholeiitic amphibolites, BIF, garnet-biotite schist (with kyanite/sillimanite/staurolite), calc-silicate and barite bearing fuchsite quartzite, layered mafic complexes
Older PGC (>3.4 Ga)			TTG, migmatites

2.3.2. Altered metabasalt (AMB)

This litho-unit is hydrothermally altered and appears as dark greyish, fine grained schistose rock (Fig. 3A and D). Albite and chlorite constitute the major mineral with subordinate ankerite (in varying proportion), sericite, quartz, minor muscovite, paragonite and tourmaline. Albite occurs as fine to medium grained laths as well as subhedral grains. Deformed grains of albite with miss-matched, bent and faulted twinning suggest brittle-ductile deformation in the area. Chlorites occur as colourless to pale greenish, flaky grains. Ankerite occurs as fine to medium, disseminated, lenticular, deformed, strained grains with kink bands.

At places the AMB appears as banded rock. The bands are composed of chlorite, albite, ankerite (15–20%) and quartz alternating with ankerite rich band/layer (ankerite ~80%) with varying proportion of chlorite and albite. Deformation twin lamellae are common in quartz grains. Minor amount of fine sericite grains are noticed both along the microlithon and cleavage domain of the foliation planes. Paragonite occurs as minor mineral. Very fine grained (<0.1 mm) tourmaline occurs as clusters within the AMB. Sphene, rutile, ilmenite and apatite are common accessory mineral with rare zircon. Dissemination of sulphides is ubiquitous. Two generations of pyrite and arsenopyrite (Fig. 3L) are noticed in the drill core samples of the AMB. The latter being the important and significant event as fine gold grains (3–4 μm) are observed in few of the second generation arsenopyrite grains. The AMB is traversed by secondary veins.

2.3.3. Greywacke and meta-argillite/phyllite

Greywacke is greyish to yellowish-grey, foliated, fine to medium grained altered litho-unit consisting of quartz, sericite, chlorite, ankerite, muscovite and chloritoid. 15–50% of the rock consists of sub-angular to sub-rounded, strained and polycrystalline quartz aggregate with serrated grain margin. Quartz clasts measure 0.8–2.2 mm in size. Sub-angular clasts dominate over the sub-rounded one. The matrix consists of very fine flakes of sericite, minor muscovite, fine and flaky chlorite and fine ankerite grains. Schistosity is noticed to warp around the quartz clasts at places. Few late tectonic, prismatic chloritoid porphyroblasts are present in the matrix. Meta-argillite is fine grained, greyish-green to brownish-green, carbonaceous rock and occurs as interband with coarse and gritty greywacke.

2.3.4. Carbonated metabasic dykes

This litho-unit is brownish grey, massive to crudely foliated, fine grained, equigranular rock consisting of altered plagioclase laths, secondary chlorite and ankerite. Minor amount of quartz grains are present. Polysynthetic twinning is noticed in some of the plagioclase grains. Clinopyroxene grains are almost completely pseudomorphed by chlorite flakes. At rare places sub-ophitic texture is preserved. Ankerite grains constitute approximately 20–50% of the rock. Euhedral pyrite grains are present.

2.3.5. Veins

Broadly four types of veins traverse the above mentioned litho-units occurring in the area in varying proportion. These are (i) ankeritic lense/vein, (ii) quartz-ankerite vein, (iii) albite-tourmaline-carbonate-quartz vein, and (iv) quartz-calcite/calcite vein. Summarized description of the different veins and their petrographic characteristics are presented in Table 2.

3. Gold mineralization and wall rock alteration

The central part of the CGB is extensively studied and numerous prospective zones of gold mineralization are reported along the NNW–SSE trending "Shear Corridor" (Khan, 2001). Amongst all the gold prospects along this "Shear Corridor", two most promising lodes (Zone-1 and 2) were delineated east of G.R.Halli village roughly along the contact of the metabasalt and meta-argillite (Khan, 2001). The zone-1 mineralization occurs in a lode with an indicated resource of 0.32 million tonnes of ore at an average grade of 3.3 g/t gold and 110 ppm Ag. In Zone-2 an inferred resource of 0.68 million tonnes of ore containing 0.4 to 8.94 g/t Au has been reported (Vasudev, 2009). Gold mineralization is intimately associated with pyrite + arsenopyrite ± pyrrhotite ± galena ± sphalerite ± chalcopyrite assemblage in whitish to smoky grey sheared quartz and minor carbonates (Khan, 2001). The prospect was explored by Hutti Gold Mines Company Limited (HGML) through two winzes, one main shaft and two adits. HGML had

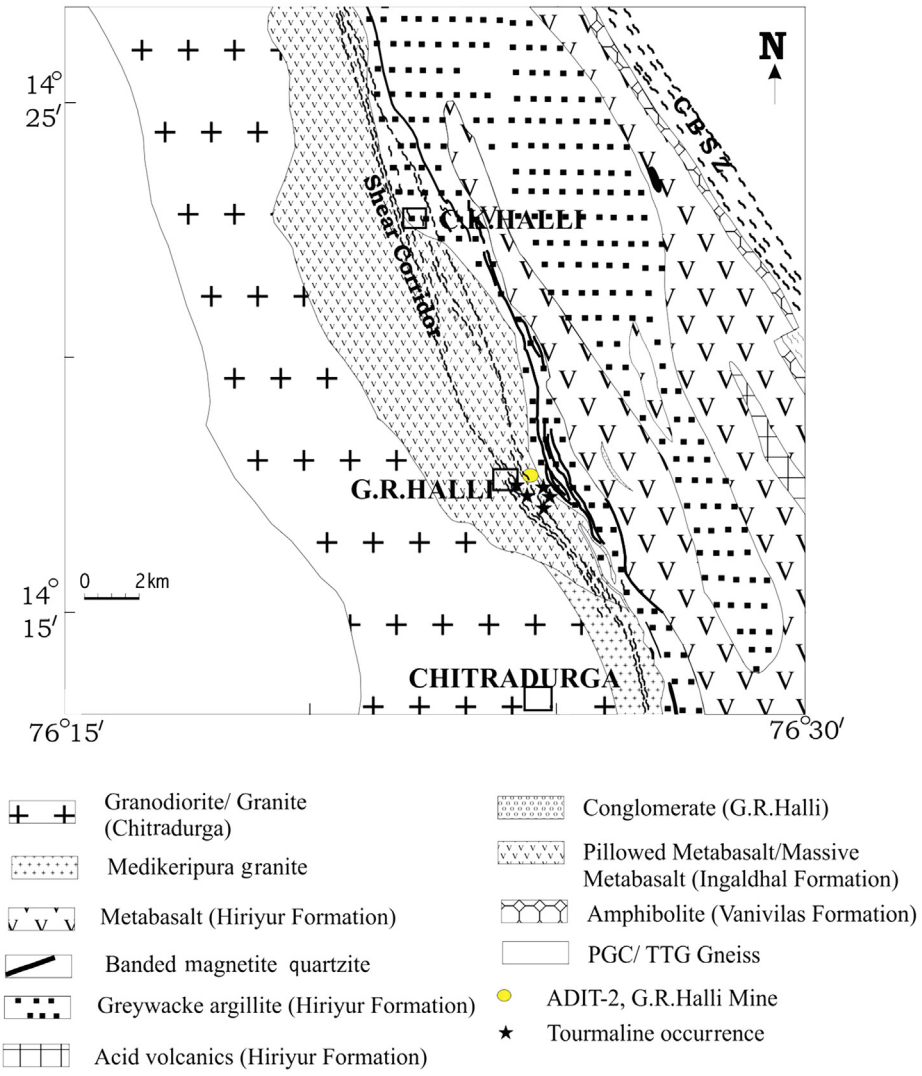

Figure 2. Simplified geological map of the study area (Khan, 2001) showing adit-1 of G.R.Halli mine and tourmaline occurrences.

established 1.3 lakh tonnes of different category of ore reserves with an average grade of 3.9 g/t. A total of 13,413 tonnes of ore was raised from the exploratory mine development (Patil, 2001), leading to exploitation of 134 kg of gold (GSI, 2012). Recently, based upon carbon and oxygen isotope data of carbonates from auriferous quartz carbonate veins magmatic/mantle source is proposed for the G.R.Halli gold deposits (Sarangi et al., 2012).

The wall rock alteration assemblage present in the alteration halo of the G.R.Halli gold mine has completely obliterated the premetamorphic mineral assemblage and to some extent the metamorphic assemblage also. Presence of tourmaline is reported in the southern and western part of the hydrothermal wall rock alteration halo of the G.R.Halli gold deposit. Previous studies indicate carbonatization, sericitization and chloritization as the common wall rock alterations developed around this gold deposit (Khan, 2001). During the present study development of wall rock alteration assemblages, from proximal to distal part of the deposit, manifested in the form of (i) quartz veins developed both in metabasalt and meta-argillite/phyllite; (ii) ankeritic lense/vein rich zones; (iii) quartz + sericite zones (iv) chlorite + ankerite + quartz + albite + Na-mica (paragonite) zones and (v) quartz + ankerite + tourmaline + albite zones are observed. Among the alteration assemblages the ankerite based alterations are most prolific and extensive in both proximal and distal parts of the mineralized zones. Such alterations occur in the form of ankeritization of the AMB and intercalated greywacke and meta-argillite/phyllite. Tourmaline bearing assemblages are mainly noticed in the AMB and ankeritic lense/vein in western and southern part of the distal wall rock alteration zone of the G.R.Halli gold deposit (Fig. 2).

4. Occurrences and compositions of tourmaline

4.1. Occurrences of tourmaline

Tourmaline from the wall rock alteration halo of the G.R.Halli gold deposit is the focus of the present study. Based upon the mode of occurrences, tourmaline has been grouped as follows:

(1) Tourmaline occurring in the AMB (Fig. 3E);
(2) Tourmaline occurring as a part of veins viz: albite-tourmaline-ankerite-quartz veins (Fig. 3F–I) and albite-tourmaline-calcite-quartz vein (Fig. 3J).

All the three types of tourmaline characteristically represent the intense hydrothermal activity in the area and are present in the

Figure 3. A–D. Field photographs showing the tourmaline bearing litho-units from the alteration halo of G.R.Halli gold deposit. A: AMB and host rock of vein-1 tourmaline in the southern part of the G.R.Halli gold deposit; B: ankeritic lense/vein in the AMB. Vein-1 tourmaline also traverse in this lense/vein (southern part of G.R.Halli gold deposit); C: AMB and host rock of vein-2 tourmaline in the western part of the G.R.Halli gold deposit; D: AMB and host rock of the AMB tourmaline. For details please refer the text. E–L. Photomicrographs showing zoning in tourmaline and inter-relationship between tourmaline and associated minerals of G.R.Halli area. Photomicrographs G and I are taken under plane polarized light whereas H and K are taken between cross nicols. E, F and J are BSE images. Photomicrograph L is taken under reflected light. E: BSE image of fine grained, prismatic AMB tourmaline (Tur) in equilibrium with the alteration assemblages of Fe-rich chlorite (Chl), quartz (Qtz), ankerite (Ank) in the AMB. Note fine arsenopyrite (Asp) grain and very thin rim in two tourmaline grains; F: prismatic tourmaline (Tur) grains in association with quartz (Qtz) in albite-tourmaline-ankerite-quartz vein (vein-1); G: basal section of tourmaline bearing albite-ankerite-quartz vein (vein-1). Note the equilibrium association of albite (Alb) and tourmaline (Tur) in quartz (Qtz) rich matrix; H: antitaxial growth of the tourmaline grains in vein-1. The median line can be traced both side along the black line; I: equilibrium association of tourmaline (Tur) and ankerite (Ank). Ankerite is partly limonitized. Note deformation twin lamellae and fluid inclusions in quartz (Qtz); J: equilibrium association of tourmaline (Tur), calcite (Cal) and quartz (Qtz) in alb-tourmaline-calcite-quartz vein (vein-2); K: deformed albite grain in albite-tourmaline-ankerite-quartz vein (vein-1); L: two generations of arsenopyrite (Asp, shown as I and II) in bore hole core sample from G.R.Halli mine area. For details please refer the text.(Continued).

distal wall rock alteration halo of the G.R.Halli gold deposit (Fig. 2). For the purpose of description the tourmaline hence forth will be referred as AMB tourmaline (tourmaline occurring in the AMB), vein-1 tourmaline (tourmaline occurring in the albite-tourmaline-ankerite-quartz veins) and vein-2 tourmaline (tourmaline occurring in the albite-tourmaline-calcite-quartz vein). Vein tourmalines stand for both vein-1 and vein-2 tourmalines. Detailed description of the different types of tourmaline is presented in Table 3.

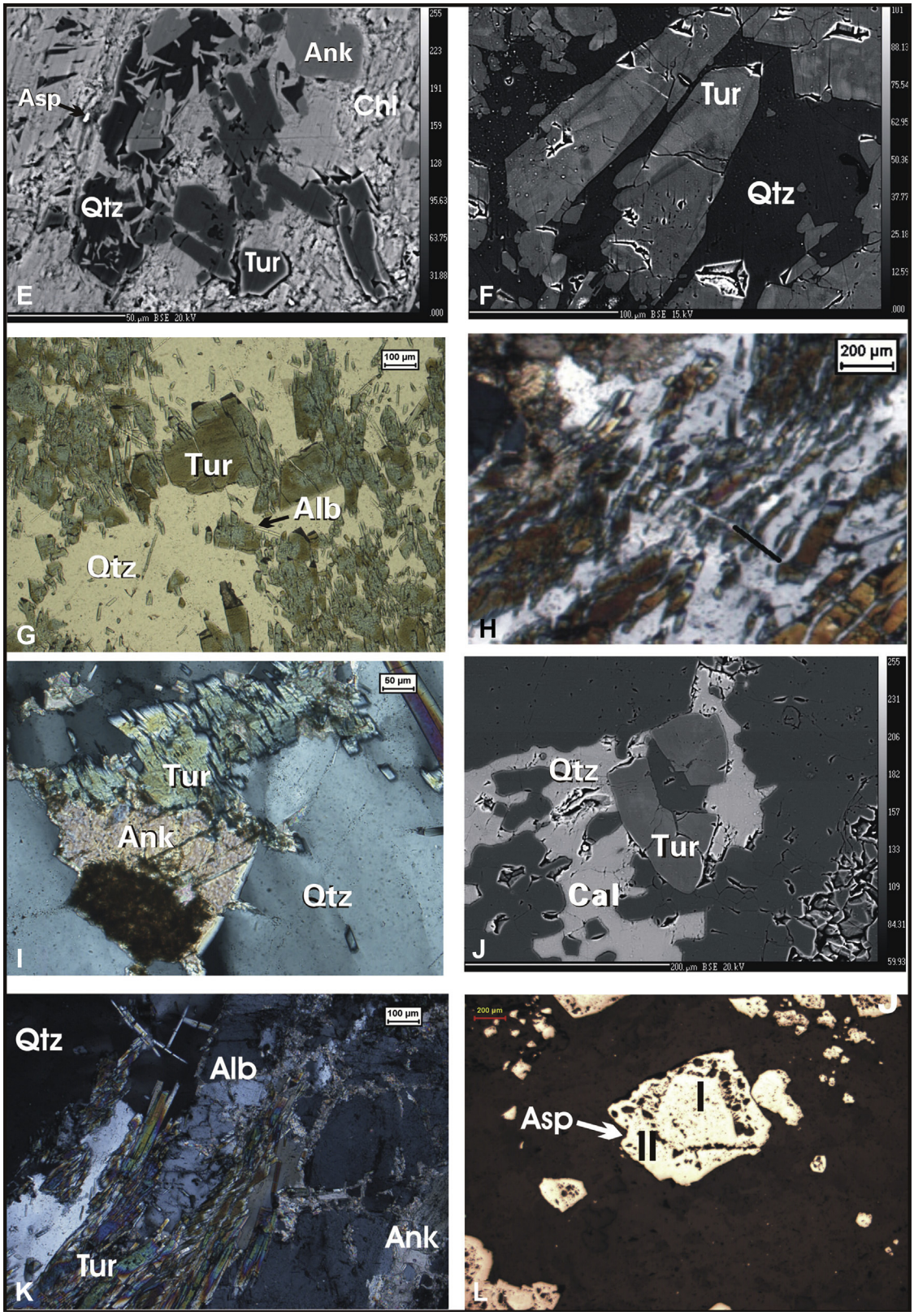

Figure 3. (*continued*).

Table 2
Different types of veins occurring in the area, their field and petrographic characteristics. Carbonate species are confirmed by EPMA study.

Vein type	Size	Outcrop	Petrography
Ankeritic lense/vein	It varies in thickness between a few cm and upto 50 m	It occurs as interband/lense/vein with elephant skin weathering. Fresh rock appears as greyish, medium grained with sheet like fracture filling quartz vein (Fig. 3B).	It consists of 70 to 90% ankerite, 5 to 25% of chlorites, quartz and minor sericite. Chlorite occurs as colourless to feebly pleochroic (pale greenish to greenish) scaly aggregates. Minute sericite flakes and few muscovite grains are noticed in these ankeritic lense/vein. Fine disseminations of pyrite and minor chalcopyrite are present.
Quartz-ankerite vein	It varies in thickness from <1 to 8 cm	Ankerite occurs in the outer margins whereas quartz forms the central parts of the vein. These quartz-ankerite veins are sulphidic at places.	Quartz occurs as flattened grains with irregular margins and fluid inclusion trails. Distinct strain shadows and neo grain development of quartz grains are noticed. Ankerite occurs as deformed, rhombic as well as irregular grains with deformation twin lamellae. At places fine chlorite and muscovite flakes are present.
Albite-tourmaline-carbonate-quartz veins	It varies in thickness between 0.5 and 2 cm	These veins are noted in AMB and ankeritic lense. It occurs either as massive or fibrous veins.	Quartz constitutes nearly 50–60% of the veins and occurs as flattened and strained grains. Carbonates are either ankerite or calcite. Tourmaline occurs as prismatic as well as long fibrous grains. Two characteristic colour zones viz. pale yellowish brown rim and bluish green core, are noticed in the tourmaline grains. Few highly deformed albite grains are seen. Discontinuous, bent and miss-matched twin lamellae are common in albite grains.
Quartz-calcite/calcite vein	It varies in thickness between 0.4 and 1.5 cm	This vein is not as common as other veins mentioned above. It occurs either as quartz-calcite vein or as pure calcite veins.	Quartz constitutes nearly 40–60% of the mode and occurs as strained grains. Calcite occurs as subhedral grains with rhombohedral cleavage and lamellar twinning.

4.2. Compositions of tourmaline

4.2.1. Analytical methods

Tourmaline was analysed quantitatively by Wavelength Dispersive Spectrometry (WDS) using CAMECA SX100 electron microprobe instrument at Petrology, Petrochemistry and Ore Dressing Division, Geological Survey of India, Bangalore. The analyses were carried out at an accelerating potential of 15 kV and 15 nA using 1 to 3 μm diameter electron beam depending up on the size and nature of the mineral. Well characterized natural and synthetic standards were used for the analytical work. The following standards were used: albite for Na, wollastonite for Si and Ca, orthoclase for Al and K, olivine for Mg, rutile for Ti, rhodonite for Mn, magnetite for Fe and apatite for P. Fluorine was not analysed. Boron, lithium and OH contents cannot be detected by electron microprobe. The content of Na was measured first for 10 s to avoid errors resulting from the volatilization. The cations and the mineral formula were calculated by using software developed by Julie Seley and Jian Xiang and supplied by Andy Tindle Free Softwares available in the net and confirmed manually. The calculation of the atomic proportion was made by assuming that boron has a stoichiometric value of 3 atoms per formula unit (apfu). Li is estimated by subtracting the sum of the Y-site cations from 3 and OH + F + Cl = 4 apfu. Both the amount of B_2O_3, necessary to produce 3 boron cations and the amount of Li_2O required to fill the deficiencies in Y-site are calculated from stoichiometry. Fe_{total} is assumed to be essentially all Fe^{2+}. The data are presented in Supplementary Table 1 (AMB tourmaline), Supplementary Table 2 (vein-1 tourmaline) and Supplementary Table 3 (vein-2 tourmaline).

4.2.2. Results

In back scattered image very thin zoning is noticed in rare AMB tourmaline grains (Fig. 3E) but no significant variation is observed in core and rim chemistry of the AMB tourmaline (Supplementary Table 1). Core and rim chemistry of the vein tourmalines are chemically different. Compositionally all the tourmalines of the G.R.Halli area are classified under alkali group tourmaline (Fig. 4A). In the Al-Fe-Mg diagram (Fig. 4B) all samples cluster in the middle of the diagram above the schorl-dravite line suggesting dominance of Al and negligible role of Fe^{3+} during the formation of tourmaline. The average Al_{total} is high and in excess of 6 apfu and it is highest in the AMB tourmaline with an average value of 6.43 apfu. The Al-saturation of the tourmaline can also be noticed when compared with Si (average Al > average Si). Despite distinct Al-enrichment, the tetrahedral Al (Al^{IV}) is either negligible or very low. The X-site in the tourmaline mainly accommodates Na^+, K^+, Ca^+ and X-site vacancy (*r*). The chemistry of both the AMB and the vein tourmalines indicates that the X-site is dominated by either Na or *r* with near absence of K and negligible amounts of Ca (average ≤ 0.03 apfu). In Mg/(Mg + Fe) vs. *r*/(Na + *r*) plot (Fig. 4C) the AMB tourmaline is classified as schorl with a tendency of crystallization towards foitite whereas the vein tourmalines are dravitic in composition. There exists a strong inverse correlation between X-site vacancy and Na_x of the AMB tourmalines and the vein tourmalines (Fig. 4D). Cores of the vein tourmalines have high X-site vacancy but low Na content than the rims. This distinction is evident in Mg_{total} vs X-site vacancy plot (Fig. 4E). In this plot, cores and rims of the vein tourmalines and the AMB tourmaline, though have variation in Mg_{total} content, exhibit similar crystallization trends but maintain distinctly different clusters. In Ti (apfu) vs Fe/(Fe + Mg) plot (Fig. 4F) rims of the vein tourmalines reflect divergent crystallization trend from their cores. Same tendency of core and rim crystallization of the vein tourmalines are noted in Ca (apfu) vs X-site vacancy plot (Fig. 4G). Slightly higher values of Ca (average value for core is 0.04 apfu and rim is 0.09 apfu) in vein-2 tourmaline may probably be related to the equilibrium association of tourmaline and calcite and diffusion of Ca into tourmaline structure.

The site-specific substitutions and vector diagrams are useful in understanding the crystallization history of tourmaline (Henry et al., 2002). Operation of each vector, in essence, indicates the actual substitution that took place during the crystallization history of the tourmaline. In Al_{total} vs X-site vacancy plot (Fig. 4H),

Table 3
Characteristics of different types of tourmaline occurring in the distal alteration halo of G.R.Halli gold deposit.

Tourmaline type		Size and type of vein	Occurrence of tourmaline	Place of occurrence with respect to G.R.Halli mine	Host rock/outcrop description	Petrography
AMB tourmaline		–	Microscopic, very fine grained (<0.1 mm) and occurs as clusters within the AMB very close to the tourmaline bearing veins (Fig. 3D).	Southern part of the G.R.Halli mine area in the distal wall rock alteration halo.	Host rock is AMB (Fig. 3A)/For outcrop description refer Section 2.3.	Tourmaline occurs as pleochroic grain and constitute minor mineral of the fine grained matrix of the host rock. Other associated minerals are Fe-rich chlorite with subordinate albite, ankerite, micaceous minerals (sericite, muscovite and paragonite) and sulphides (mainly pyrite and arsenopyrite.
Vein tourmaline	Vein-1 tourmaline	Veins vary in thickness from 2 to 2.5 cm and grown in discontinuity with the country rock & perpendicular to the vein wall. These veins are identified as antitaxial veins where growth occurred from inside out. The growth of the fibres of tourmaline in these veins occurs along a median line visible in the thin sections (Fig. 3H).	Megascopic. Tourmaline occurs as black, prismatic crystals and developed like comb texture perpendicular to wall rock.	Southern part of the G.R.Halli mine area in the distal wall rock alteration halo.	Host rock is AMB (Fig. 3A) and ankeritic lense or vein (Fig. 3B)/ For outcrop description refer Section 2.3 and Table 2.	Tourmaline occurs as fibrous, elongated as well as prismatic grains (Fig. 3F–H). The elongated tourmaline grains measure upto 1.3 cm. Distinct bluish core and brownish rim is present in these tourmaline grains. The boundary between the core and rim is sharp. Few of the tourmaline fibres are kinked. The tourmaline grains occur in equilibrium with ankerite (Fig. 3I) and albite (Fig. 3G). The close association of the tourmaline with ankerite indicates the hydrothermal origin of the former. Quartz constitutes nearly 55–60% of the vein and occurs as lobate, flattened and strained grains. Both subgrain and neo grain developments are noticed along and across the flattening in quartz grains. Ankerites occur as rhombic euhedral as well as subhedral grains. Few highly deformed albite occurs as platy grains with deformed twin lamellae (Fig. 3K).
	Vein-2 tourmaline	Veins vary in thickness from few mm to 1.4 cm and grown in discontinuity with the AMB country rock.	Megascopic and occurs as stubby, prismatic grains.	Western part of the G.R.Halli mine area in the distal wall rock alteration halo.	Host rock is AMB (Fig. 3C)/For outcrop description refer Section 2.3.	Tourmaline occurs as prismatic grains (Fig. 3J). It is strongly pleochroic with bluish-green core and brownish rim. Quartz occurs as subhedral, strained grains whereas calcite grains are noticed in equilibrium with the prismatic tourmaline grains. Few deformed albite grains are present.

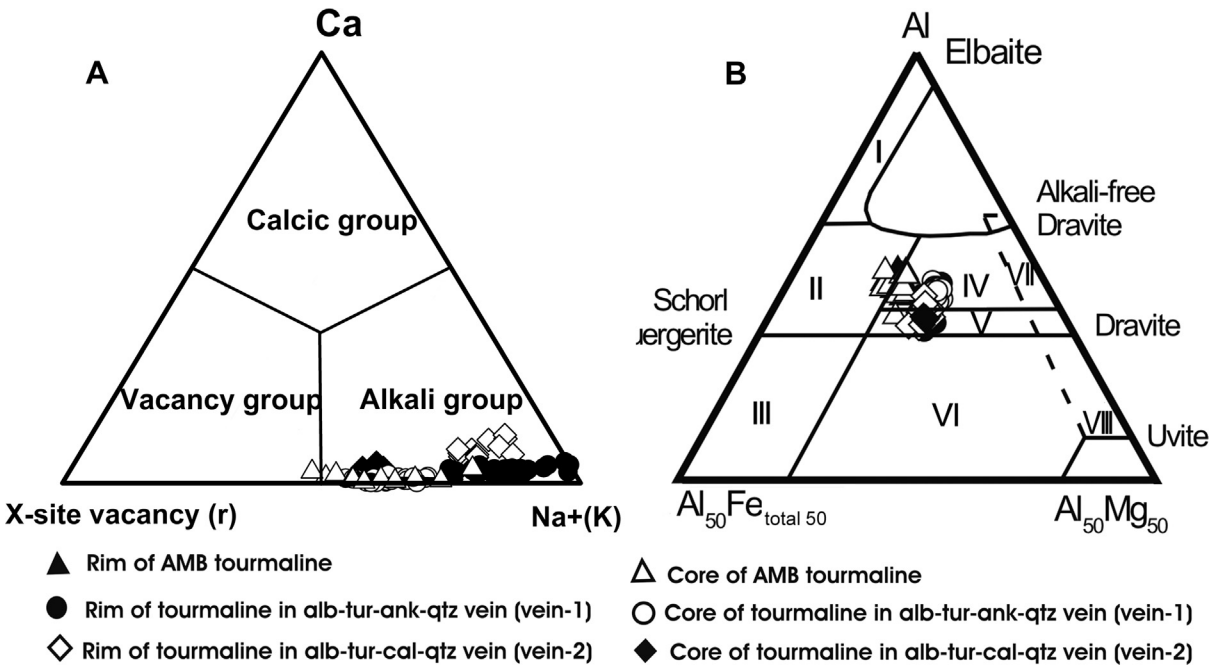

Figure 4. A–B. A: Ternary diagram using electron microprobe data classify the tourmaline (after Hawthorne and Henry, 1999) based upon the major alkali minerals in the X-site. Note that all the analysed tourmaline of the G.R.Halli area plot in the alkali-group field. B: Al-Fe-Mg ternary diagram (after Henry and Guidotti, 1985) using electron microprobe data for the tourmaline of G.R.Halli area. Different regions in the diagram represent compositional range of tourmaline from different rock types. Abbreviations used in the diagram are defined as: I. Li-rich granitoid, pegmatites and aplites; II. Li-poor granitoids, pegmatites and aplites; III. Fe^{3+}-rich quartz-tourmaline rocks (hydrothermally altered granites); IV. Metapelites and metapsammites co-existing with an Al-saturating phase; V. Metapelites and metapsammites not co-existing with Al-saturating phase; VI. Fe^{3+}-rich quartz-tourmaline rocks, calc-silicates and meta-pelites; VII. Low-Ca meta-ultramafic and Cr, V-rich meta-sediments and VIII. Meta-carbonates and meta-pyroxenites. C–F. Ratio and inter-cation correlation diagram of AMB, vein-1 and vein-2 tourmaline showing clear distinction between AMB, core and rim tourmaline chemistry. C: Mg/(Mg + Fe) vs r/(Na + r) plot; D: Na_x (apfu) vs X-site vacancy (r) plot; E: Mg (apfu) vs X-site vacancy (r) plot; F: Ti (apfu) vs Fe/(Fe + Mg) plot. Symbols used are same as in A and B. G–I. Inter-cation correlation diagram of AMB, vein-1 and vein-2 tourmaline showing distinct clusters of three types of tourmaline. G: Ca (apfu) vs X-site vacancy (r) plot; H: Al_{total} (apfu) vs X-site vacancy (r) plot; I: Mg (apfu) vs Fe_{total} (apfu) plot. Note in G and H, AMB and core of the vein tourmalines cluster roughly together. Symbols used are same as in A and B.(Continued).

operation of rAl(Na,R)−1 vector is evident (where R = Fe + Mg + Mn) for the tourmalines of G.R.Halli area. Combining both Fe vs Mg plot (Fig. 4I) and Al_{total} vs X-site vacancy plot, the influence of rAl(Na,R)−1 can be confirmed. This suggests that both the AMB tourmalines and the vein tourmalines had excess X-site vacancy and Al that were replaced by Na and R cations. But in the Fe_{total} vs Mg diagram (Fig. 4I) operation of two distinct exchange vectors are evident i.e. rAl(Na,Fe)−1 for the vein tourmalines and MgFe−1 for the AMB tourmaline. The exchange vector rAl(Na,Fe)−1 is much similar to the one observed in X-site vacancy and Na_x plot (Fig. 4D).

5. Discussion

Gold occurrences, whether economically viable or not, are discovered in many greenstone belts of most Achaean cratons (Groves and Batt, 1984; Goldfarb et al., 2001 and references therein). Quartz-carbonate veins hosted Archean lode gold mineralization with in shear zones, faults, extentional veins, breccias constitutes one of the most important types of mesothermal or orogenic gold ore deposits (Cameron, 1988; Barnicoat et al., 1991; Ho et al., 1992). The hydrothermal origin for the orogenic gold deposit of the Archean greenstone belt is globally accepted. In hydrothermal systems, tourmaline develops as a consequence of infiltration of boron-bearing hydrothermal fluids and can have a wide range of compositions depending upon the bulk composition of the host lithologies and the invasive fluids (Taylor and Slack, 1984; Cavarrette and Puxedda, 1990; Henry and Dutrow, 1996; Fareeduddin et al., 2010). Being a sensitive indicator of the environment in which each of its mineral species crystallize (Garba, 1996), the tourmaline abundance and its chemistry reflect the dominant influence of either the host rocks (if boron rich fluids are subordinates) or the hydrothermal system (if the fluids are enriched in boron). Slack (1996) documented that many vein-type metal deposits, especially gold-bearing deposits in metamorphic terrain, contain tourmaline as a component of the vein or an alteration mineral in adjacent wall rock and most of these deposits fall in the category of mesothermal, shear zone hosted (orogenic) gold ores. Tourmaline generally occurs as a minor gangue mineral within the vein and/or in wall rocks and rarely it constitutes a significant portion of the ores. In many gold deposits, tourmaline formed contemporaneously and is paragenetically related to gold mineralization, while in other deposits it is unrelated to mineralization.

The detailed petrography and chemical analyses have brought out some similarities and distinctions between the AMB tourmaline and the vein tourmalines. In the vein tourmalines zoning, with blue core and brown rim having sharp boundary, is distinct compared to the AMB tourmaline. The AMB tourmaline and the vein tourmalines are alkali group tourmaline with dominance of Na and near absence of K and Ca having an alumina-saturated chemistry. However, it is observed that the composition of the AMB tourmaline and cores of the vein tourmalines are similar, whereas rims of the vein tourmalines have different mineral chemistry. The schrol tourmaline (AMB tourmaline) and cores of the dravitic tourmaline (vein tourmalines) exhibit remarkable similarities in terms of abundance of monovalent and divalent cations in X and Y sites and their inter-relations, which implies common conditions of formation for the AMB tourmaline and cores of the vein tourmalines. The AMB tourmaline occurs very close to the tourmaline bearing veins traversing through

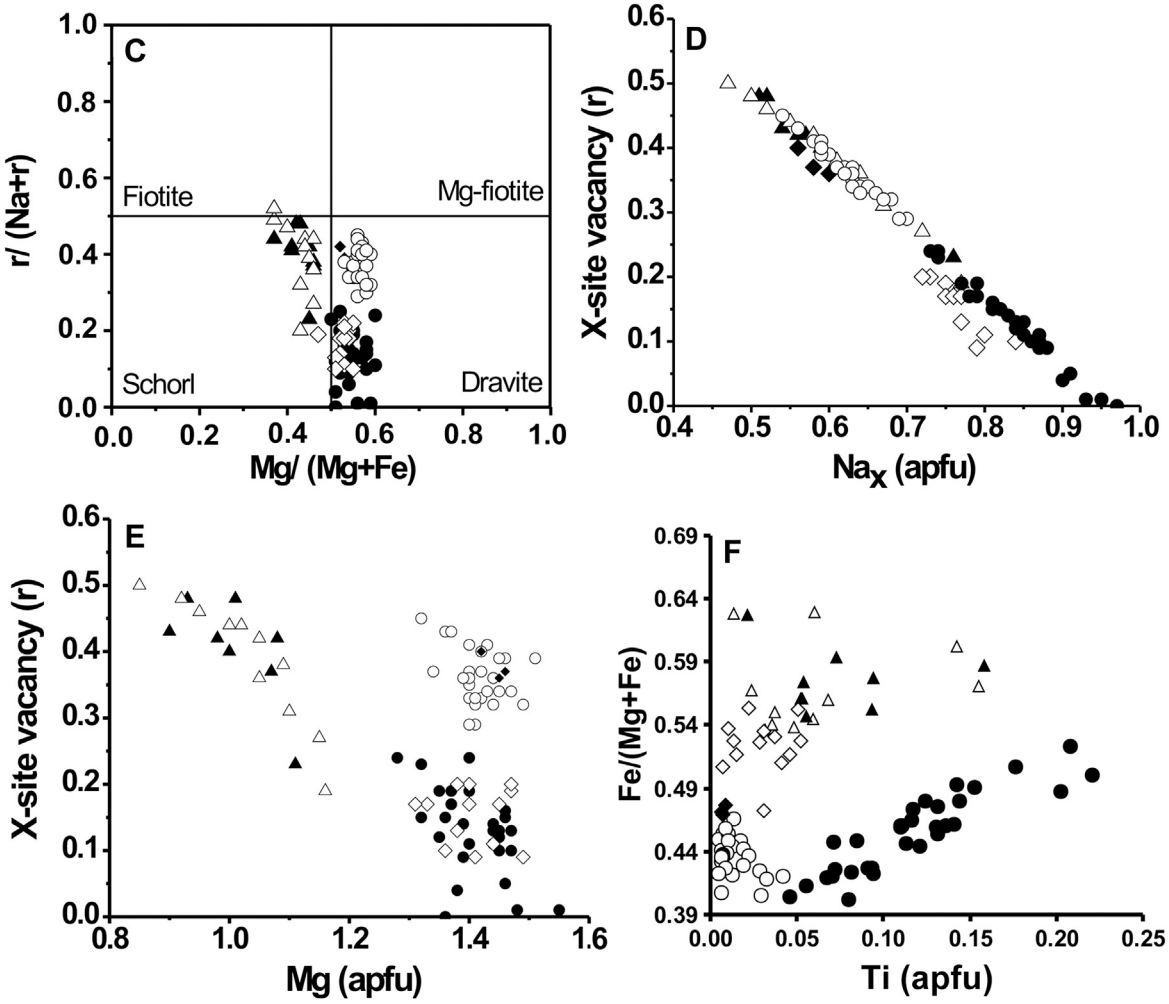

Figure 4. (*continued*).

the host AMB. Based upon the chemical similarities between the AMB tourmaline and cores of the vein tourmalines it is concluded that cores of the vein tourmalines and by implication the AMB tourmaline are formed from the same fluid during the same event. The composition of rims of the vein tourmalines not only get clustered differently in most binary discrimination diagrams but also have different trend of crystallization. The crystallization trends of rims of the vein tourmalines either do not follow the same trend as that of their cores (Mg vs X-site vacancy diagram, Fig. 4E) or maintain almost divergent crystallization trend as in Ti vs Fe/(Mg + Fe) plot (Fig. 4F) and Ca vs X-site vacancy plot (Fig. 4G). The inverse relation between rims and cores chemistry with respect to Al^{IV} and X-site vacancy, different crystallization trends and presence of sharp contact between cores and rims (implying lack of progressive transition from core to rim as expected in normal single phase crystallization) suggest that cores and rims of the vein tourmalines do not share a common crystallization history and therefore represent two events of tourmaline crystallization. Host rock influence remaining the same, the above mentioned difference could probably be due to change in the fluid chemistry during crystallization of the vein tourmalines from core to rim. This change is the fluid chemistry is also documented in the intra-grain traverse map of vein-1 (Fig. 5A–F) and vein-2 tourmalines (Fig. 6A–F). In both vein-1 and vein-2 tourmalines, there is sharp increase of TiO_2, MgO, CaO and Na_2O from core to rim whereas reverse tendency is noted for FeO^T and $r/(Na + r)$ ratio. Rims of the vein tourmalines, therefore, crystallized after the formation of the AMB tourmaline and cores of the vein tourmalines. The cationic substitutions are subsequent to the crystallization of schrol (AMB tourmaline) and dravite (vein tourmalines) and possibly dictated by the host rock lithology. Iron substitution for magnesium is dominant in the AMB tourmaline (Mg being the major component in the basalt) whereas R and Na substitutions for Al and X-site vacancy respectively are dominant in the vein tourmalines (Fig. 4H and I).

5.1. Condition of tourmaline formation

Henry and Dutrow (1996) observed that (i) there is a general increase in the calculated Al^{IV} of tourmaline with the increasing grade of metamorphism; (ii) there is little or no Al^{IV} below 450 °C, but it progressively increases up to an average of 0.25 apfu above 750 °C; and (iii) in the same tourmaline, X-site vacancies decrease from 0.6 ± 0.2 to 0.30 ± 0.05 as temperature increases from 200 to 650 °C with further decrease to 0.05 ± 0.05 above 750 °C. The average X-site vacancy and Al^{IV} of different types of tourmaline of G.R.Halli area are summarized in Table 4. The average Al^{IV} for all the tourmalines of the area varies between zero and 0.03 apfu, which suggests their formation temperature to be below 450 °C. The average X-site vacancy for the AMB tourmaline and cores of the vein tourmalines are 0.40 and 0.37 respectively whereas for rims it is 0.14, which imply their temperature of formation to be between 200 and 650 °C. From the above parameters it is deduced that (i)

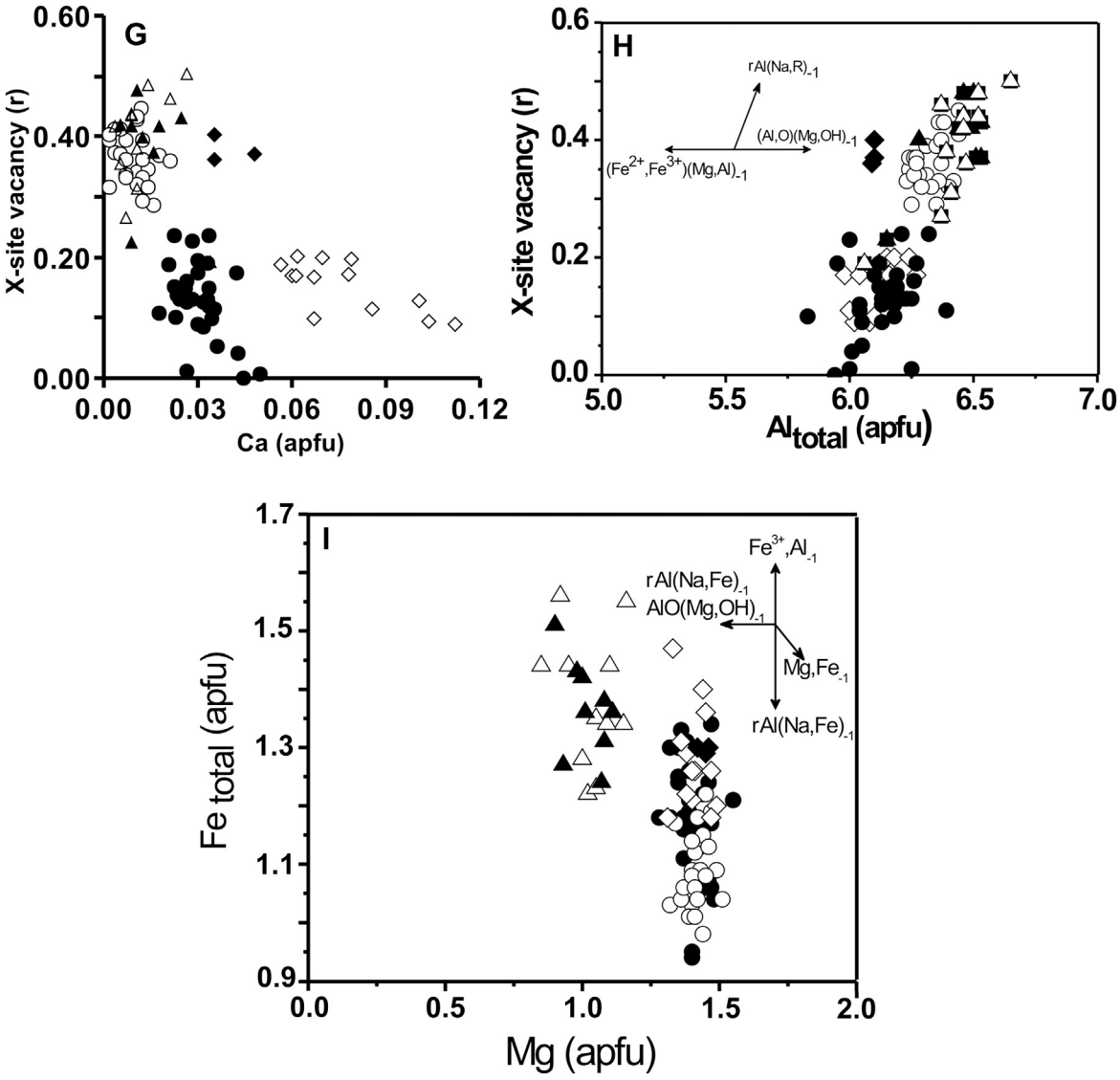

Figure 4. (*continued*).

the AMB tourmaline and cores of the vein tourmalines and (ii) subsequently gold mineralization and rims the vein tourmalines have crystallized between 200 and 450 °C. The X-site vacancy of rims of the vein tourmalines is less than their cores and inversely related to Na_x (apfu) (Fig. 4D). It suggests that higher temperature prevailed during the formation of rims of the vein tourmalines. This can be corroborated with the regional high temperature-low pressure (HT-LP) tectonothermal event, which was associated with shearing vis-à-vis mineralization in the Dharwar craton. The amount of Na in the X-site is not only temperature dependent, but also a function of co-existing aqueous phases (Von Goerne et al., 2001). The Na content of rims is more than cores in the vein tourmalines of G.R.Halli area. This in turn is related to the gradual increase of Na content in the mineralized hydrothermal fluid. Presence of Na mica i.e. paragonite in the alteration zone (Gupta and Fareeduddin, 2013) also confirms the role of Na rich fluids during the formation of rims of the vein tourmalines.

5.2. Tourmaline development and regional geological scenario

Published Sm-Nd whole rock isochrones of metabasalts as well as U-Pb zircon ages of felsic volcanics suggest the time frame work of greenstone volcanism in central part of the CGB is between 2740 and 2670 Ma (Nutman et al., 1992; Anil Kumar et al., 1996; Jayananda et al., 2011a, b, 2013). In the studied area the CGB is intruded by high-potassic Chitradurga granite pluton in the west, Jampalnaikankote (J.N. Kote) pluton to the east and Maddakkanahalli granite and tonalitic Sira flat gneiss in the southeast. The Chitradurga pluton is emplaced during the regional D_1 deformation, synkinematic with development of dome-basin pattern in the WDC and show superimposed deformation patterns as revealed by post-emplacement mafic dykes which are deflected towards the CBSZ along the eastern part of the present study area (Jayananda et al., 2006). On the other hand J.N. Kote granodioritic to tonalitic pluton in the eastern part of the CGB is affected by regional shear zone network (D_2 event) as reflected in the CBSZ. SIMS U-Pb zircon ages indicate 2614 ± 10 Ma for Chitradurga granite (Jayananda et al., 2006). Though J.N. Kote pluton has not been dated, however, immediately southeast the tonalitic flat gneiss provide SHRIMP U-Pb zircon age of 2559 ± 5 Ma and Maddakkanahalli pluton found in flat gneiss indicate 2507 ± 5 Ma age (Chardon et al., 2011). It is likely that J.N. Kote pluton emplaced within the time frame work of 2560–2507 Ma during the end Achaean tectonothermal event. Nd isotope data of the Chitradurga granite suggests its derivation by

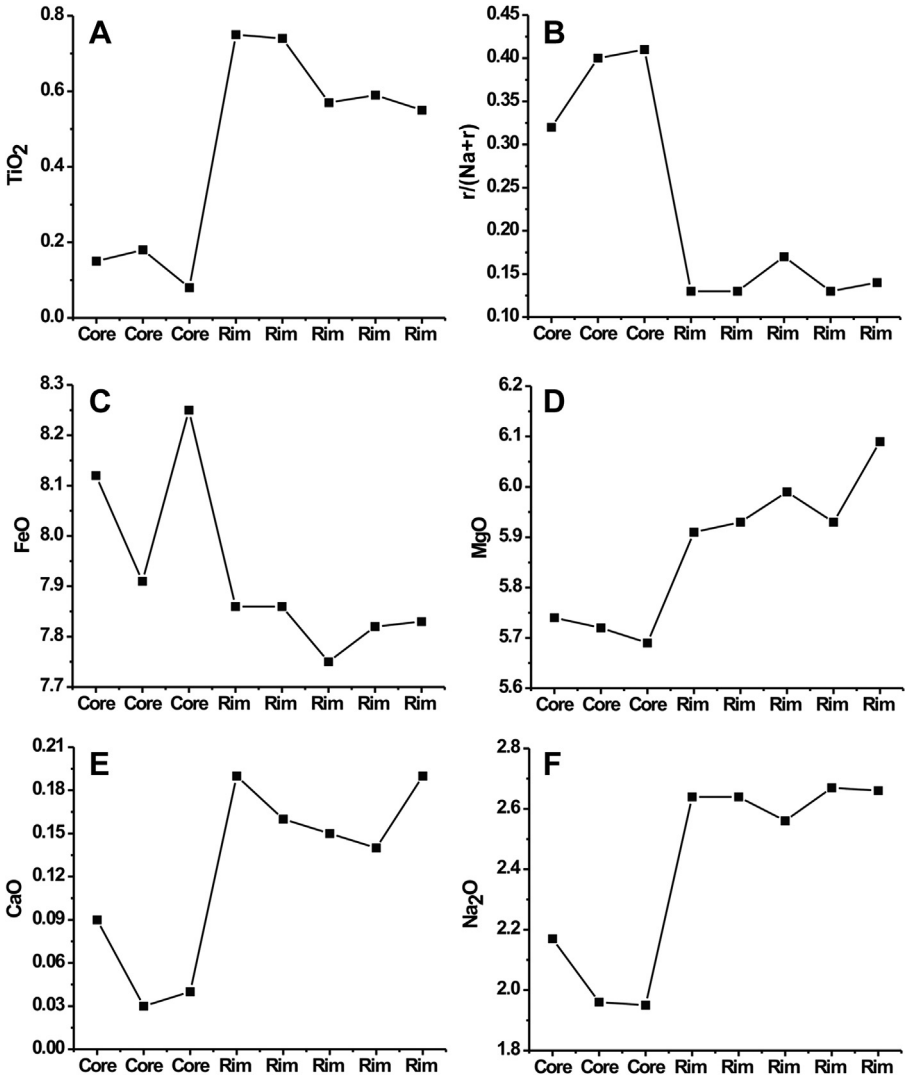

Figure 5. A–F. Binary plots [TiO_2, r/(Na + r), FeO, MgO, Na_2O and CaO] representing intra-grain variation from core (76.4 μm) to rim (74.7 μm) of a single tourmaline grain (size 151.1 μm) of albite-tourmaline-ankerite-quartz vein (vein-1 tourmaline) of G.R.Halli area. Note the sharp change from core to rim values in all the plots. (Detection points are shown Supplementary Table 2. Rim data are detection points 1/1, 2/1, 3/1, 4/1 and 5/1 and core data are detection points 6/1, 7/1 and 8/1).

reworking of ancient deep crustal TTG basement with mantle input representing the final regional Archean plutonic event in the WDC (Jayananda et al., 2006). The deformation, metamorphism (greenschist to lower amphibolites facies) and fluid flows associated with the pluton emplacements are well preserved in the present study area. Consequently it appears that the fluid flow associated ca. 2.61 Ga Chitradurga granite caused the formation of the AMB tourmaline and cores of the vein tourmalines of G.R.Halli area.

The granitoids of the EDC are regionally distributed, mainly juvenile and emplaced between 2.55 and 2.51 Ga in a context of pervasive strike-slip shearing, (Jayananda et al., 2006) which has been linked with the gold mineralization in the Dharwar craton during D_2 deformational event in Gadag area (Sarma et al., 2008, 2011). As already noted in situ SIMS zircon U-Pb dating of the Sira tonalitic flat gneiss and the Maddakkanahalli pluton near the study area in the eastern part of the CBSZ has provided ages of 2559 ± 4 Ma and 2507 ± 5 Ma respectively (Chardon et al., 2011). These juvenile magmatic accretions and associated shear deformation, fluid flow and HT-LP metamorphism (Chardon and Jayananda, 2008; Jayananda et al., 2013) probably caused growth of rims of the vein tourmalines in G.R.Halli area. This second event of regional deformation, metamorphism and fluid flow might have caused the gold mineralization in G.R.Halli and other regions including Ajjanahalli in the CGB and Gadag (Sarma et al., 2008, 2011; Sarangi et al., 2012).

Our present study correlates well with the regional scenario discussed above and we propose that the formation of the AMB tourmaline and cores of the vein tourmalines is related to the D_1 deformation event, pluton emplacement and fluid flow in the WDC around 2.61 Ga. Rims of the vein tourmalines vis-à-vis gold mineralization in G.R.Halli area formed subsequently from mineralized hydrothermal fluids released during the 2.56–2.50 Ga accretion event in the western part of the EDC. The signature of these two regional events are also registered in the two generations of pyrite and arsenopyrite (Fig. 3L) observed in the bore hole sample of the G.R.Halli gold deposit suggesting two phases of fluid influx, the younger of these two is associated with the gold mineralization in the area.

Ajjanahalli and Gadag gold deposits occur in close proximity of the CBSZ in northern and southern part of G.R.Halli respectively. In situ U-Pb dating of monazite and xenotime in gold reefs of the Gadag (2522 ± 6 Ma) and Ajjanahalli (2520 ± 9 Ma) gold deposits reveal 2.52 Ga gold mineralization event, which is the youngest of all dated events and only one gold mineralization event in this part

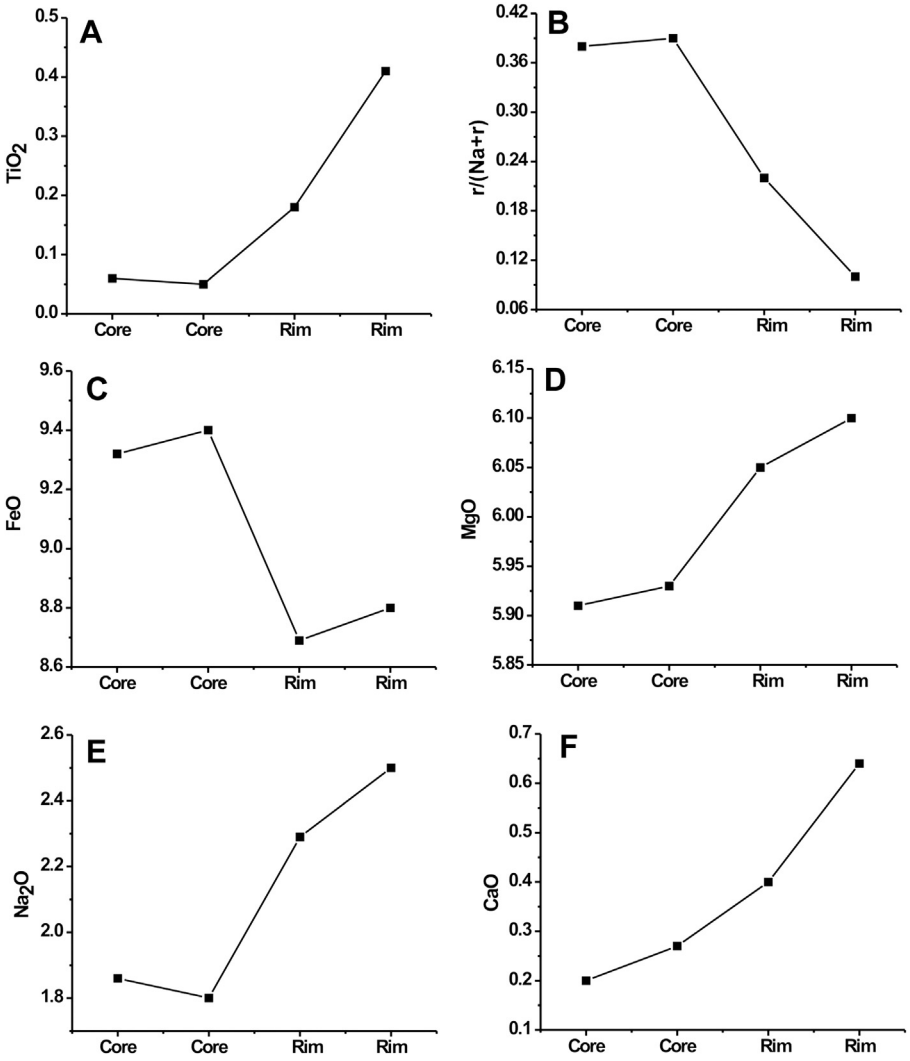

Figure 6. A–F. Binary plots [TiO_2, r/(Na + r), FeO, MgO, Na_2O and CaO] representing intra-grain variation from core (64.5 μm) to rim (76.8 μm) of a single tourmaline grain (size 141.3 μm) of albite-tourmaline-calcite-quartz vein (vein-2) of G.R.Halli area. Note increase in the TiO_2, MgO, Na_2O and CaO content form core to rim whereas FeO content and r/(Na + r) ratio decrease from core to rim. (Detection points are shown in Supplementary Table 3. Rim data are detection points 12/1 and 13/1 and core data are detection points 10/1 and 11/1).

of the WDC (Sarma et al., 2011). The G.R.Halli gold deposit occurs in the shear zone (Khan, 2001; Mohakul and Babu, 2001; Chadwick et al., 2007) and in proximity to the CBSZ. It is therefore presumed that the gold mineralization event in G.R.Halli is contemporary to the other two deposits.

5.3. Implication of boron rich fluid sources

The two most important factors for tourmaline formation from hydrothermal fluids are (i) source of the hydrothermal fluids and (ii) source of boron. The generation of hydrothermal boron involves diverse crustal processes such as seafloor spreading, subduction, felsic magmatism, volcanism and metamorphic devolatilization (Slack, 1996; Ram Mohan et al., 2008). Dewatering of the protolith during progressive metamorphism can effectively remove boron from the metasedimentary rocks (Moran et al., 1992). Boron is mobile in most aqueous solution which acts to concentrate or disperse it (Slack, 1996). Boron contents in the mafic rock are very low whereas metasedimentary rocks are the most important source of boron (Harder, 1970). Due to low Fe and Mg content in most granitoids, they are not able to conserve boron as tourmaline in the crystallizing melt (London and Manning, 1995). The boron-rich magmatic and hydrothermal fluids exsolved from granitoid melts and expelled into the surrounding country rock and formed minor to abundant tourmaline where sufficient Fe and/or Mg and Al are available for its formation (Manning, 1981; Morgan and Landon, 1987; London and Manning, 1995). Boron loss in metamorphic rock can involve boron partitioning into fluids generated by dehydration reaction or into invasive fluids. Boron enrichment in the rock is also achieved where boron bearing hydrothermal or metamorphic fluids interacts with the host rock (Slack, 1996). It is therefore interpreted that boron bearing hydrothermal fluids released during the regional D_1 deformation event and granitoid

Table 4
Average X-site vacancy and Al^{IV}(apfu) of different types of tourmaline occurring in the alteration halo of G.R.Halli gold deposit.

Tourmaline type	Average X-site vacancy	Average Al^{IV}
AMB tourmaline	0.40	0.03
Vein-1 tourmaline	Core: 0.36	0
	Rim: 0.13	0.03
Vein-2 tourmaline	Core: 0.38	0
	Rim: 0.15	0

plutonism (2.61 Ga events) close to the study area in the WDC has resulted in the development of the AMB tourmaline and cores of the vein tourmalines. The boron bearing auriferous hydrothermal fluids released during the 2.56–2.50 Ga juvenile magmatic accretion in arc setting in the western part of the EDC are probably responsible for the formation of rims of the vein tourmalines vis-à-vis gold mineralization in G.R.Halli area.

6. Summary and conclusions

The conclusions of the present study are summarized as follows:

(1) Tourmaline is a minor but important mineral in the distal wall rock alteration halo of the G.R.Halli gold deposit.
(2) Tourmaline of the G.R.Halli area is grouped as AMB tourmaline and vein tourmalines (vein-1 and vein-2). The AMB tourmaline is devoid of any significant zoning whereas the vein tourmalines are zoned. The AMB tourmaline and cores of the vein tourmalines are contemporary and older whereas rims of the vein tourmalines are younger and co-genetically related to gold mineralization of the area.
(3) Boron bearing hydrothermal fluids, released during the emplacement 2.61 Ga Chitradurga granite pluton in the WDC, resulted in the development of cores of the vein tourmalines and the AMB tourmaline. Formation of rims of the vein tourmalines vis-à-vis gold mineralization in the G.R.Halli area are resulted from mineralized hydrothermal fluids released during the 2.56–2.50 Ga juvenile magmatic accretion in arc setting in the western part of the EDC.
(4) Tourmaline formed from boron bearing hydrothermal fluids with available Fe and Mg content of the host rock. The required alumina for the formation of the tourmaline might have been leached from the metasedimentary litho-units interlayered with the metabasalt in the area.
(5) Based upon the average Al^{IV} and X-site vacancy of tourmaline of the area it is concluded that the AMB tourmaline plus cores of the vein tourmalines and rims of the vein tourmalines vis-à-vis gold mineralization formed between 200 and 450 °C, the younger mineralizing fluid having a relatively higher temperature.

Acknowledgement

The authors are thankful to the Deputy Director General, Geological survey of India, NER, Shillong for granting permission to publish the paper. The work pertains to the field season programme (2008–09) of GSI. Thanks are due to the colleagues of GSI for their help, guidance and fruitful discussion at various stages of the investigation. We also thank Mahesh Korakoppa (GSI) for help in EPMA analytical work. We appreciate the critical comments, suggestions and recommendations of anonymous reviewers which helped to substantially improve the earlier version of the manuscript.

Appendix A. Supplementary data

Supplementary data related to this article can be found at http://dx.doi.org/10.1016/j.gsf.2013.12.004.

References

Anil Kumar, Rao, B., Sivaraman, Y.J., Gopalan, K., 1996. Sm-Nd ages of Archean metavolcanics of the Dharwar craton, South India. Precambrian Research 80, 205–216.
Barnicoat, A.C., Fare, R.J., Groves, D.I., McNaughton, N.J., 1991. Synmetamorphic lode-gold deposits in high-grade Archean settings. Geology 19, 921–924.
Bhaskar Rao, Y.J., Sivaraman, T.V., Pantulu, C.V.C., Gopalan, K., Naqvi, S.M., 1992. Rb-Sr ages of late Archean metavolcanics and granites, Dharwar craton, south India and evidence for early Proterozoic thermotectonic event(s). Precambrian Research 59, 145–170.
Cameron, E.M., 1988. Archean gold: relation to granulite formation and redox zoning in the crust. Geology 16, 109–112.
Cavarrette, G., Puxedda, M., 1990. Schorl-dravite-ferridravite tourmaline deposited by hydrothermal magmatic fluids during early evolution of the Larderello geothermal field, Italy. Economic Geology 85, 1236–1251.
Chadwick, B., Vasudev, V.N., Hegde, G.V., 1997. The Dharwar craton, southern India and its late Archean Plate Tectonic settings: current interpretations and controversies. Proceedings of the Indian Academy of Sciences: Earth and Planetary Sciences 106 (4), 249–258.
Chadwick, B., Vasudev, V.N., Hegde, G.V., 2000. The Dharwar craton, southern India interpreted as a result of Late Archean oblique convergence. Precambrian Research 99, 91–111.
Chadwick, B., Vasudev, V.N., Hegde, G.V., Nutman, A.P., 2007. Structure and SHRIMP U/Pb zircon ages of granites adjacent to the Chitradurga Schist Belt: implications for Neoarchean convergence in the Dharwar craton, southern India. Geological Society of India 69, 5–24.
Chardon, D., Jayananda, M., 2008. Three dimensional field perspective on deformation, flow and growth of the lower continental crust (Dharwar craton, India). Tectonics 27, TC1014. http://dx.doi.org/10.1029/2007TC002120.
Chardon, D., Jayananda, M., Peucat, J.J., 2011. Lateral constrictional flow of hot orogenic crust: insights from the Neoarchean of south India, geological and geophysical implications for orogenic plateaux. Geochemistry Geophysics Geosystems 12, 1–24.
Dey, S.M., 2013. Evolution of the Archean crust in the Dharwar craton: the Nd isotope record. Precambrian Research 227, 227–246.
Drury, S.A., Holt, R.W., Van Calastern, P.C., Beckinsale, R.D., 1983. Sm-Nd and Rb-Sr ages for Archean rocks in western Karnataka, South India. Journal of the Geological Society of India 24, 454–460.
Fareeduddin, Gupta, S., Golani, P.R., Kirmani, I.R., Chander, S., 2010. Tourmaline as metallogenic indicator: examples from Paleo-Proterozoic Pb-Zn and Cu-Au deposits of Rajasthan, India. Journal of the Geological Society of India 76, 215–243.
Garba, I., 1996. Tourmalinization related to Late Proterozoic-Early Palaeozoic lode gold mineralization in the Bin Yauri area, Nigeria. Mineralium Deposita 31, 201–209.
Goldfarb, R.J., Groves, D.I., Gardoll, D., 2001. Orogenic gold and geologic time: a global synthesis. Ore Geology Reviews 18, 1–75.
Groves, D.I., Batt, W.D., 1984. Spatial and temporal variations of Archean metallogenic associations in terms of evolution of granitoid-greenstone terrains with particular emphasis on the western Australian Shield. In: Kroner, A., Hanson, G.N., Goodwin, A.M. (Eds.), Archean Geochemistry, pp. 73–98.
GSI, 2012. Training Course on Geological Mapping in Granite-Greenstone Terrain Around Chitradurga. www.portal.gsi.gov.in.
Gupta, S., Fareeduddin, 2013. Occurrence of paragonite in the hydrothermal wall rock alteration zone of G.R.Halli gold deposit, Chitradurga Schist Belt, Western Dharwar Craton, southern India. Journal of the Geological Society of India 82, 461–473.
Harder, H., 1970. Boron content in sediments as a tool in facies analysis. Sedimentary Geology 4, 153–157.
Hawthorne, F.J., Henry, D.J., 1999. Classification of the minerals of the tourmaline group. European Journal of Mineralogy 11, 201–216.
Henry, D.J., Dutrow, B.L., 1996. Metamorphic tourmaline and its petrologic applications. In: Grew, E.S., Anovitz, L.M. (Eds.), BORON: Mineralogy, Petrology and Geochemistry. Reviews in Mineralogy, vol. 33, pp. 503–557.
Henry, D.J., Guidotti, C.V., 1985. Tourmaline as a petrogenetic indicator mineral: an example from the staurolite-grade metapelites of NW Maine. American Mineralogist 70, 1–15.
Henry, D.J., Dutrow, B.L., Silverstone, J., 2002. Compositional asymmetry in replacement tourmaline – an example from the Tauern Window, Eastern Alps. Geological Materials Research 2, 1–18.
Ho, S.E., Groves, D.I., McNaughton, N.J., Miicki, E.J., 1992. The source of ore fluids and solutes in Archean lode gold deposits of western Australia. Journal of Volcanology and Geothermal Research 50, 173–196.
Hodgson, C.J., 1993. Mesothermal lode gold deposits. In: Kirkham, R.V., Sinclair, W.D., Thorpe, R.I., Duke, J.M. (Eds.), Mineral Deposit Modeling. Geological Association of Canada Special Paper, vol. 40, pp. 635–678.
Hutchinson, R.W., 1993. A multi-stage, multi-process genetic hypothesis for greenstone-hosted gold lodes. Ore Geology Reviews 8, 349–382.
Jayananda, M., Moyen, J.F., Martin, H., Peucat, J.-J., Aurvay, B., Mahabaleswar, B., 2000. Late Archean (2550–2520 Ma) juvenile magmatism in the EDC, southern India: constraints from geochronology, Nd-Sr isotopes and whole rock geochemistry. Precambrian Research 99, 225–254.
Jayananda, M., Chardon, D., Peucat, J.-J., Capdevila, R., 2006. 2.61 Ga potassic granites and crustal reworking in the WDC, Southern India: tectonic, geochronological and geochemical constraints. Precambrian Research 150, 1–26.
Jayananda, M., Kano, T., Peucat, J.-J., Channabasappa, S., 2008. 3.35 Ga komatiite volcanism in the western Dharwar craton, southern India: constraints from Nd isotopes and whole-rock geochemistry. Precambrian Research 162, 160–179. http://dx.doi.org/10.1016/j.precamres.2007.07.010.
Jayananda, M., Banerjee, M., Pant, N.C., Dasgupta, S., Kano, T., Mahesha, N., Mahabaleshwar, B., 2011a. 2.62 Ga high temperature metamorphism in the

central part of the eastern Dharwar craton: implications for late Archean tectonothermal history. Geological Journal 46. http://dx.doi.org/10.1002/gj.1308.

Jayananda, M., Jahn, Bor-ming., Gireesh, R.V., Bora, S., 2011b. Geochronologic and isotopic constraints on accretionary relationships of western and eastern blocks of the Dharwar craton across Huliyar and Sira corridor: implications for late Archean tectonics. In: International Symposium on Precambrian Accretionary Orogens and Field Workshop in the Dharwar Craton. Geological Society of India, pp. 51–54.

Jayananda, M., Peucat, J.-J., Chardon, D., Krishna Rao, B., Corfu, F., 2013. Neoarchean greenstone volcanism, Dharwar craton, Southern India: constraints from SIMS zircon geochronology and Nd isotopes. Precambrian Research 227, 55–76. http://dx.doi.org/10.1016/j.precamres.

Khan, S.A., 2001. Gold mineralization along Gonur-Jagalur shear corridor in central part of the Chitradurga schist belt, Karnataka. In: National Seminar on Exploration and Survey for Noble Metals and Precious Stones. Geological Survey of India, Special Publication, vol. 58, pp. 251–261.

Krienitz, M.S., Trumbull, R.B., Hellmann, A., Kolb, J., Meyer, F.M., Wiedenbeck, M., 2008. Hydrothermal gold mineralization at the Hira Buddini Gold Mine, India: constraints on fluid sources and evolution from boron isotopic compositions of tourmaline. Mineralium Deposita 43 (4), 421–434.

London, D., Manning, D.A.C., 1995. Chemical variation and significance of tourmaline from southwest England. Economic Geology 90, 495–519.

Manning, D.A.C., 1981. The application of experimental studies in determining the origin of topaz-quartz-tourmaline rocks and tourmaline-quartz rock. Proceedings of the Ussher Society 5, 121–127.

Mohakul, J.P., Babu, P.H., 2001. Granitoid hosted gold mineralization in Honnamaradi prospect, Chitradurga schist belt, Karnataka. Geological Survey of India, Special Publication 58, 263–270.

Moran, A.E., Sisson, V.B., Leeman, W.P., 1992. Boron depletion during progressive metamorphism: implication for subduction processes. Earth and Planetary Science Letters 111, 331–349.

Morgan, G.B., Landon, D., 1987. Alteration of amphibolite wall rock around the Tanco rare element pegmatite, Bernic Lake, Manitoba. American Mineralogist 772, 1097–1121.

Mukhopadhyay, D., 1986. Structural pattern in the Dharwar craton. Journal of the Geological Society of India 94, 167–186.

Mukhopadhyay, D., Baral, M.C., 1985. Structural geometry of the Dharwar rocks near Chitradurga. Journal of the Geological Society of India 26, 547–566.

Mukhopadhyay, D., Ghosh, D., 1983. Superposed deformation in Dharwar rocks of the southern part of the Chitradurga schist belt, Karnataka. In: Naqvi, S.M., Rogers, J.J.W. (Eds.), Precambrian of South India. Memoirs of the Geological Society of India, vol. 4, pp. 275–292.

Mukhopadhyay, D., Baral, M.C., Ghosh, D., 1981. A tectono-stratigraphic model of the Chitradurga schist belt, Karnataka, India. Journal of the Geological Society of India 22, 22–31.

Naqvi, S.M., 1985. Chitradurga schist belt- an Archean suture? Journal of the Geological Society of India 26, 511–525.

Nutman, A.P., Chadwick, B., Ramakrishnan, M., Viswanatha, M.N., 1992. SHRIMP U-Pb ages of detrital zircon in Sargur supracrustal rocks in western Karnataka, southern India. Journal of the Geological Society of India 39, 367–374.

Patil, M.L., 2001. Evolutionary phases of exploration leading to the development of Hutti and Chitradurga group of mine in the Archean Greenstone Belt of Karnataka, India. In: National Seminar on Exploration and Survey for Noble Metals and Precious Stones. Geological Survey of India, Special Publication, vol. 58, pp. 293–314.

Peucat, J.-J., Jayananda, M., Chardon, D., Capdevila, R., Fanning Marc, C., Paquette, Jean-Louis, 2013. The lower crust of Dharwar craton, south India: patchwork of Achaean granulitic domains. Precambrian Research, 1–25. http://dx.doi.org/10.1016/ j.precamres.

Raase, P., Raith, M., Ackermand, D., Lal, R.K., 1986. Progressive metamorphism of mafic rocks from greenschist facies to granulite facies in the Dharwar craton of southern India. Journal of Geology 94, 261–282.

Radhakrishna, B.P., Curtis, L.C., 1999. Gold in India. Journal of the Geological Society of India, 308.

Radhakrishna, B.P., Vaidhyanadhan, R., 2011. Geology of Karnataka. Geological Society of India, 353 p.

Ram Mohan, M., Kamber, Balz S., Piercey, S.J., 2008. Boron and Arsenic in highly evolved felsic rocks: implications for Achaean subduction processes. Earth and Planetary Science Letters 27, 479–488.

Roberts, R.G., 1987. Archean lode gold deposits. Geoscience Canada 14, 37–52.

Rollinson, H.R., Windley, B.F., Ramakrishnan, M., 1981. Contrasting high and intermediate pressures of metamorphism in the Archean Sargur Schists of southern India. Contributions to Mineralogy and Petrology 76, 420–429.

Sarangi, S., Sarkar, A., Srinivasan, R., Patel, S.C., 2012. Carbon isotope studies of auriferous quartz carbonate veins from two orogenic gold deposits from the Neoarchean Chitradurga schist belt, Dharwar craton, India: evidence for mantle/magmatic source of auriferous fluid. Journal of Asian Earth Sciences 52, 1–11.

Sarma, D.S., Mc Naughton, N.J., Fletcher, I.R., Groves, D.I., Ram Mohan, M., Balaram, V., 2008. The timing of gold mineralization of Hutti gold deposit, Dharwar craton, South India. Economic Geology 103, 1715–1727.

Sarma, D.S., Fletcher, I.R., Rasmussen, B., McNaughton, N.J., Ram Mohan, M., Groves, D.I., 2011. Archean gold mineralisation of the western Dharwar craton, India: 2.52 Ga U-Pb ages of hydrothermal monazite and xenotime in gold deposits. Mineralium Deposita 46, 273–288.

Sheshadri, T.S., Chaudhuri, A., Harinadha Babu, P., Chayapathi, N., 1981. Chitradurga schist belt. Memoirs of Geological Survey of India 112, 328 p.

Siva Siddaiah, N., Rajamani, V., 1989. The geologic setting, mineralogy, geochemistry and genesis of gold deposits of the Archean Kolar schist belt, India. Economic Geology 84, 2155–2172.

Slack, J.F., 1996. Tourmaline associations with hydrothermal ore deposits. In: Grew, E.S., Anovitz, L.M. (Eds.), BORON: Mineralogy, Petrology and Geochemistry. Reviews in Mineralogy, vol. 33, pp. 559–643.

Swami Nath, J., Ramakrishnan, M., 1981. Early Precambrian supracrustals of Southern Karnataka. Memoirs of Geological Survey of India 112, 328 p.

Swami Nath, J., Ramakrishnan, M., Viswanatha, M.N., 1976. Dharwar stratigraphic model and Karnataka craton evolution. Records of the Geological Survey of India 107, 149–175.

Taylor, B.E., Slack, J.F., 1984. Tourmaline from Appalachian-Caledonian massive sulphide deposits: textural, chemical and isotopic relationships. Economic Geology 79, 1703–1726.

Vasudev, V.N., 2009. Field guide to selected gold prospects in Karnataka and Andhra Pradesh. In: National Seminar on Gold Industry in India. Geological Society of India, pp. 19–20.

Von Goerne, G., Franz, G., Heinrich, W., 2001. Synthesis of tourmaline solid solutions in the system Na_2O-MgO-Al_2O_3-SiO_2-B_2O_3-H_2O-HCl and the distribution of Na between tourmaline and fluid at 300 to 700 degrees C and 200 MPa. Contributions to Mineralogy and Petrology 141, 160–173.